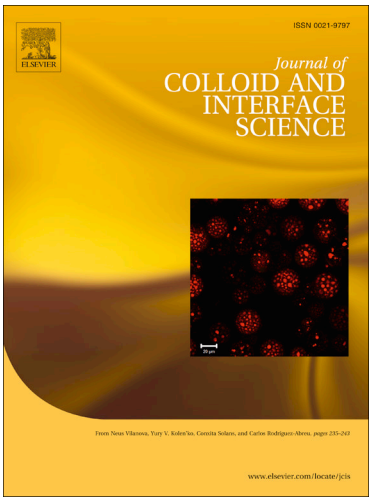

The contact angle of nanofluids as thermophysical property

M. Hernaiz, V. Alonso, P. Estellé, Z. Wu, B. Sundén, L. Doretti, S. Mancin, N. Çobanoğlu, Z.H. Karadeniz, N. Garmendia, M. Lasheras-Zubiate, L. Hernández López, R. Mondragón, R. Martínez-Cuenca, S. Barison, A. Kujawska, A. Turgut, A. Amigo, G. Huminic, A. Huminic, M.-R. Kalus, K.-G. Schroth, M.H. Buschmann

PII: S0021-9797(19)30422-9
DOI: https://doi.org/10.1016/j.jcis.2019.04.007
Reference: YJCIS 24836

To appear in: *Journal of Colloid and Interface Science*

Received Date: 27 November 2018
Revised Date: 1 April 2019
Accepted Date: 3 April 2019

Please cite this article as: M. Hernaiz, V. Alonso, P. Estellé, Z. Wu, B. Sundén, L. Doretti, S. Mancin, N. Çobanoğlu, Z.H. Karadeniz, N. Garmendia, M. Lasheras-Zubiate, L. Hernández López, R. Mondragón, R. Martínez-Cuenca, S. Barison, A. Kujawska, A. Turgut, A. Amigo, G. Huminic, A. Huminic, M.-R. Kalus, K.-G. Schroth, M.H. Buschmann, The contact angle of nanofluids as thermophysical property, *Journal of Colloid and Interface Science* (2019), doi: https://doi.org/10.1016/j.jcis.2019.04.007

The contact angle of nanofluids as thermophysical property

M. Hernaiz[1], V. Alonso[1], P. Estellé[2], Z. Wu[3], B. Sundén[3], L. Doretti[4], S. Mancin[5], N. Çobanoğlu [6], Z.H. Karadeniz[7], N. Garmendia[8], M. Lasheras-Zubiate[8], L. Hernández López[9], R. Mondragón[9], R. Martínez-Cuenca[9], S. Barison[10], A. Kujawska[11], A. Turgut[12], A. Amigo[13], G. Huminic[14], A. Huminic[14], M.-R. Kalus[15], K.-G. Schroth[16], M.H. Buschmann*,[16]

[1] *Surface Chemistry and Nanotechnology Unit, IK4-Tekniker, C/Iñaki Goenaga 5, 20600 Eibar, Spain*

[2] *Univ Rennes, LGCGM, EA3913, F-35000 Rennes, France*

[3] *Department of Energy Sciences, Lund University, P.O. Box 118, Lund SE-22100, Sweden*

[4] *Department of Civil, Architectural and Environmental Engineering, University of Padova, Via Venezia 1, 35131, Padova, Italy*

[5] *Department of Management and Engineering, University of Padova, Str.lla S. Nicola 3, 36100, Vicenza, Italy*

[6] *İzmir Kâtip Çelebi University, Graduate School of Natural and Applied Sciences, 35620, İzmir, Turkey*

[7] *İzmir Kâtip Çelebi University, Department of Mechanical Engineering, 35620, İzmir, Turkey*

[8] *NAITEC- Automotive and Mechatronics Centre. C/ Tajonar, 20, 31006 Pamplona, Navarra, Spain*

[9] *Departamento de Ingeniería Mecánica y Construcción, Universitat Jaume I, Castelló de la Plana 12071, Spain*

[10] *ICMATE - CNR, Corso Stati Uniti 4, 35127 Padova, Italy*

[11] *Wrocław University of Science and Technology, Department of Mechanical and Power Engineering, Wybrzeże St. Wyspiańskiego 27, 50-370 Wrocław, Poland*

[12] *Dokuz Eylül University, Mechanical Engineering Department, 35397, İzmir, Turkey*

[13] *Applied Physics Department, University of Santiago de Compostela, 15782 Santiago de Compostela, Spain*

[14] *Transilvania University of Brasov, Mech. Eng. Department, 29 Bulevardul Eroilor, 500036, Braşov, Romania*

[15] *Particular GmbH, Lise-Meitner-Straße 9, 31303 Burgdorf, Germany*

[16] *Institut für Luft- und Kältetechnik gGmbH Dresden, 01309 Dresden, Germany*

* Corresponding author: PD Dr.-Ing. habil. Matthias H. Buschmann
Institut für Luft- und Kältetechnik Dresden gGmbH
Bertolt Brecht Alle 20
01139 Dresden (GERMANY)
Tel.: 0049 351 4081 669
Fax: 0049 351 4081 655
Matthias.Buschmann@ilkdresden.de

Abstract

Droplet volume and temperature affect contact angle significantly. Phase change heat transfer processes of nanofluids – suspensions containing nanometre-sized particles – can only be modelled properly by understanding these effects. The approach proposed here considers the limiting contact angle of a droplet asymptotically approaching zero-volume as a thermophysical property to characterise nanofluids positioned on a certain substrate under a certain atmosphere.

Graphene oxide, alumina, and gold nanoparticles are suspended in deionised water. Within the framework of a round robin test carried out by nine independent European institutes the contact angle of these suspensions on a stainless steel solid substrate is measured with high accuracy. No dependence of nanofluids contact angle of sessile droplets on the measurement device is found. However, the measurements reveal clear differences of the contact angle of nanofluids compared to the pure base fluid.

Physically founded correlations of the contact angle in dependency of droplet temperature and volume are obtained from the data. Extrapolating these functions to zero droplet volume delivers the searched limiting contact angle depending only on the temperature. It is for the first time, that this specific parameter, is understood as a characteristic material property of nanofluid droplets placed on a certain substrate under a certain atmosphere. Together with the surface tension it provides the foundation of proper modelling phase change heat transfer processes of nanofluids.

Keywords: round robin test, contact angle, nanofluids, influence of volume, influence of temperature, experimental strategy

Nomenclature

Symbols

$a_{0,fl}$, $a_{t,fl}$, $a_{V,fl}$	coefficients, [°, ° °C^-1, ° m^-1]
k	thermal conductivity, [W (m K)^-1]
r_{dr}	droplet radius
R_a	mean roughness [m]
t	temperature, [°C]
V	volume of droplet, [µl]

Greek letters

Γ	line tension, [kg m s^-2]
γ_{lv}	liquid-vapour surface tension, [kg s^-2]
η	dynamic viscosity, [kg m^-1 s^-1]
θ	contact angle, [°]
ρ	density, [kg m^-3]
ω	frequency [s^-1]

Subscripts

ad	advancing
cor	correlation
dr	droplet
exp	experimental
fl	fluid
H2O	DI-water
nf	nanofluid
re	receding
0	under zero-volume condition

Abbreviations

CA	contact angle
DI	deionised
GO	graphene oxide
NF	nanofluid

RH	relative humidity

Abbreviations of participating institutions

IK4	IK4 TEKNIKER (Spain)
IKCU	İzmir Kâtip Çelebi University (Turkey)
ILK	Institut für Luft- und Kältetechnik Dresden (Germany)
NAITEC	NAITEC- Automotive and Mechatronics Centre (Spain)
UJI	Universitat Jaume I (Spain)
UoB	Transilvania University of Brasov (Romania)
UoL	Lund University (Sweden)
UoP	University of Padova (Italy)
UR1	Université Rennes 1 (France)
USdC	University Santiago de Compostela (Spain)
DEU	Dokuz Eylül University (Turkey)

1. Introduction

Nanofluids – suspensions containing particles with sizes ranging from 10 to 100 nm – seem to be a promising new option to increase heat transfer. Production, characterisation, and thermodynamical tests are underway to prepare these special fluids for industrial applications [1]. Determination of thermophysical properties – density, viscosity, thermal conductivity etc. – are most important for this process. This study presents a strategy to define the contact angle of nanofluids on solid surfaces and atmospheres relevant for industrial applications.

The contact angle of a nanofluid θ is the angle between the tangents on the gas-suspension interphase and on the gas-substrate interphase at the three-phase contact line [2]. Besides surface tension, the contact angles which nanofluid droplets form with substrates are among the thermophysical properties which have not yet been intensely investigated [3]. Nevertheless, the analysis of a few studies [4–7] (see Table A1 of Supplementary Material) reveals already the complexity of such an endeavour.

A nanofluid is not just another type of liquid with more or less changed thermophysical properties. In general, suspensions like nanofluids have to be considered as two-phase materials consisting of a solid component, i.e. the nanoparticles, and a liquid component, i.e. the base fluid. In flowing, nanofluids exert, with respect to their magnitude, very unequal forces (e.g. viscosity and inertia) on the nanoparticles. Hence, a single-phase character and, therewith, effective thermophysical properties may be acceptable for these flows [8]. This might not be the case in nanofluid volumes like droplets utilised for contact angle measurements which are not moving or only slowly. The decoupled movement of nanoparticles and base fluid may create e.g. ring stains following from capillarity flow [9] or a structural disjoining pressure [10].

Experiments utilising conventional devices for measuring contact angle, which is mostly the case, cannot identify such effects. Therefore, a robust experimental approach which delivers reliable results is needed. This study which is part of the NANOTENSION [14] project of the COST Action 15119 NANOUPTAKE (see COST Action NanoUptake website [1]) aims for such a strategy. It presents the results of the first Round Robin Test about contact angle measurement of nanofluids which involves nine European institutions.

The goal of this investigation is to carefully measure contact angles of well-defined nanofluids employing a solid substrate made of stainless steel as relevant surface for industrial applications. The study is performed employing different measurement techniques, as well as both commercial and in-house built devices. This variety allows to proof if contact angle measurements are affected by interdependencies between measurement device and nanofluid. Moreover, it enables to collect statistics from independent laboratories for a

massive data base which allows the development of a strategy for determining the contact angle of nanofluids.

The results are analysed with respect to plausibility and to reliability of the measurement techniques employed. In addition, recommendations are developed for the measurement and practical analysis of nanofluid contact angles. Finally, it is demonstrated that the limiting contact angle for zero-volume is the relevant thermophysical property to properly characterise a nanofluid droplet placed on a certain solid substrate under a certain atmosphere. This parameter depends on the temperature, the surface energy of the substrate, the solid-liquid interfacial interaction and the specification of the nanofluid. In case of heterogeneous nanofluids, contact angles are additionally dependent on the type of particles, their size distribution and concentrations, and possible interactions with the solid (specific adsorption, aggregation, deposition etc.).

2. Materials and methods

The three nanofluids employed in the study were produced in one batch each. Production took place simultaneously in January 2018. After production, the three batches were sent to ILK, split into nine charges, and sent together with the solid stainless steel substrate to the participants on Feb. 2nd, 2018. Figure 1 shows the three nanofluids and Fig. 2 the substrate upon posting.

2.1 Nanofluids

2.1.1 Graphene oxide nanofluid

Graphene oxide nanofluid is prepared at the Institute of Electronic Materials Technology (ITME) in Warsaw (Poland) through a modified Hummers' method. Graphite, as a source material, is oxidised at the temperature of 50 ºC in a solution of 95% sulfuric acid (10 g of graphite per 1 litre), sodium nitrate (mass ratio of sodium nitrate to graphite 2:3), and potassium permanganate (mass ratio of 6:1). The resulting slurry is diluted in deionised water and then H_2O is added. Afterwards, cleaning is performed in a microfiltration device. Finally, the solution is diluted to the graphene oxide concentration of 0.1 g/l. No surfactant is added. It is expected that the main dimensions of the graphene oxide particles ranges between 770 and 900 nm. However, their thickness is only between approximately 2 and 10 nm nanometres [18]. According to the definition of nanofluids given in the introductory section the graphene oxide nanofluid does strictly speaking not belong to this group of suspensions. However, due to practical reasons and the common practice employed in literature the GO suspension is termed nanofluid as well.

2.1.2 Alumina nanofluid

The alumina nanofluid is produced at ICMATE - Institute of Condensed Matter Chemistry and Technologies for Energy (Padua, Italy). Deionised water (Millipore, Billerica MA, 18.2 MΩ, USA) is used as base fluid. Al_2O_3 powder (Alfa Aesar, 99.5 %, 40-50 nm declared size) is dispersed in water at 0.1 vol. % concentration by combined magnetic stirring and sonication. The sonication is performed by an ultrasonic processor (VCX130, SONICS®, SONICS & MATERIALS INC., USA) at 65 W and 20 kHz for 30 min, followed by a sonication at 120 W and 20 kHz for 10 min. A Zetasizer Nano ZS (Malvern Instruments Ltd©, United Kingdom) is used to measure the average size of the nanoparticles in water and the Zeta potential. The mean size is 123 ± 2 nm and the Zeta potential 69 ± 1 mV. No surfactant is added.

2.1.3 Gold nanofluid

The gold nanofluid is produced by Particular GmbH (Germany). The nanoparticles are prepared by pulsed laser ablation directly in the base fluid DI-water (PLAL) [19]. For that purpose a gold substrate (Agosi Allgemeine Gold- und Silberscheideanstalt AG, Germany) with a purity of 99.99% and a thickness of 0.5 mm is placed in an ablation chamber filled with 100 ml Milli-Q water. Sodium chloride (NaCl, purity ≥ 99.9%, VWR Prolabo, Germany) is added prior to ablation with a concentration of 0.1 mmol/l in order to stabilise and quench the size of the gold nanoparticles [20]. Employing a Nd:YAG ns-Laser (Rofin Powerline E20, ROFIN-SINAR Laser GmbH, Germany) with working wavelength, pulse duration, repetition rate, and pulse energy of 1064 nm, 7 ns, 15 kHz, and 0.35 mJ, respectively, an intense laser beam is focussed onto the gold target. For this a F-Theta lens with a focal length of 100 mm is utilised. The spot size on the target after ablation is 40±5 µm in diameter, leading to a laser fluence of 27.9 J/cm^2. For maximal target utilisation the laser beam is guided along the gold surface according to a predefined spiral pattern with an internal diameter of 6 mm and a scan speed of 4 m/s by a galvanometric scanner (SCANcube10, SCANLAB, Germany). The nanoparticle mass concentration of the produced gold colloid is obtained by weighing the gold target before and after ablation. By adjusting the ablation time and diluting the gold colloid, a final nanoparticle mass concentration of 10 mg/l is prepared. The colloid is characterised by dynamic light scattering (Nicomp 380 DLS-ZLS, Particle Size System Inc., USA) directly after synthesis. The mean diameter of the nanoparticles is 8.34 nm (σ = 2.21 nm).

2.2 Solid stainless steel substrate

The solid substrate is made of stainless steel (Fig. 2). The dimensions of the cubic bloc are 30 mm by 30 mm, with a thickness of 5 mm. All solid substrates are manufactured from one single round stock. Substrate after substrate is cut off from this raw material utilising the same lathe to ensure the same material and surface quality of all substrates. The cube shape is obtained by milling off the sides. For the dynamic Wilhelmy plate experiments carried out by UoB, a stainless steel plate (UoB-sample) is provided which is 10 mm wide, 20 mm long, and 0.8 mm thick.

The steel material is 1.4301 N° AISI/ASTM 304 (short name X5CrNi18-10), a commonly employed stainless steel with a density of 7.9 g/cm³, a thermal conductivity of 15.0 W/(m K), and a specific heat capacity of 500 J/(kg K) at 20 °C [23]. A cast analysis delivers a typical composite of 17.00 to 19.00 % chromium, 8.00 to 10.50 % nickel, ≤ 0.07 % carbon, ≤ 1.00 % silica, ≤ 2.00 % magnesium, ≤ 0.045 phosphor, ≤ 0.015 sulphur, and ≤ 0.11 nitrogen [24]. The stainless steel plate (UoB-sample) employed for the Wilhelmy plate experiments is of the same material.

Figure 2 shows the front side of the stainless steel solid substrate on which the droplets are positioned. The visible surface structure follows from lathing. The manufacturing process creates a narrow spiral which, after light polishing, has a mean roughness index of $R_a \approx 0.20$ μm and an averaged surface roughness of 1.4 μm (see Table A2 of Supplementary Material) employing a Perthometer M4Pi (ILK, measurements according to [25]). To ensure comparable experimental conditions in each experiment, the droplets are either placed centric or at several positions on the solid substrate. In the latter case, the data which are processed further are averaged.

2.3 Measurement of contact angle

The following sections describe the measurement devices and techniques employed by the nine teams for contact angle determination. All experiments have been carried out under atmospheric pressure. In general, all experiments follow the best practice of the different institutes. For experimental details with respect to droplet size, ambient temperature, pressure (if available), and relative humidity of surrounding air see Table A3 of the Supplementary Material.

2.3.1 Biolin Scientific – Attension Theta Optical Tensiometer (IKCU)

Contact angle is measured employing an Attension Theta Optical Tensiometer (Biolin Scientific, Sweden/Finland) utilising sessile drop method. The shape of the drop on the solid substrate is analysed by images taken by a high resolution FireWire camera (1984x1264 pixel) with telecentric optic and 55 mm focus length. The camera is combined with a NAVITAR - 1-60135 zoom system (NAVITAR, NY/USA) with 6.5X zoom and 12 mm fine focus capability. The duration of each measurement is 10 s, during which 125-140 images are analysed. The drop shape is fitted to the Young-Laplace equation. In order to measure contact angles, surface tension is also measured and set as a property for each fluid.
During measurements for all fluids, the baseline, which is defined as the horizontal line connecting both three-phase points, is set up automatically by the device. Before each measurement, the solid substrate is cleaned to avoid the effects of nanoparticles on the surface roughness.

2.3.2 Krüss Goniometer G1, UJI-device (UJI)

The contact angle is determined by the sessile drop technique either employing a Krüss Goniometer G1 (Krüss Goniometer G1, Krüss GmbH, Germany) or an in-house built device.
Employing the Krüss Goniometer, droplets of known volume are positioned at the centre of the surface of the substrate using a syringe. To reduce the influence of droplet evaporation, the measurements are taken within 60 s after droplet deposition. As the equipment requires visual inspection to evaluate the contact angle, three independent observers monitor this parameter permanently. The average contact angle is calculated as the arithmetic mean of five droplets. For each droplet, the results from the three observers are considered.
The main components of the self-designed optical device are shown in Fig. 3. A horizontal platform supports a holder on which the substrate is placed. A micrometer carrier controls the height and the axial position of the droplet regulator which holds the syringe. The syringe places a sessile droplet of a certain volume onto the centre of the substrate. The apparatus has a LED panel light source, which produces a homogeneous background illumination with negligible thermal influence, thus providing an ideal contrast for the image to be taken by the camera. In this device, both contact angle and droplet volume were obtained by image processing. The images of the droplets are taken immediately after deposition to minimise a possible evaporation impact. For each fluid, the results from 3 to 6 different drops are averaged.

2.3.3 DSA-30 Drop Shape Analyzer (UR1)

Contact angle measurements at UR1 are carried with a DSA-30 Drop Shape Analyzer (KRÜSS GmbH, Germany) employing the sessile drop method. First, calibration and measurement uncertainty are checked using sessile drop gauges, with known contact angles of 30°, 60°, and 120°, respectively, provided by the manufacturer. A maximum relative deviation of 0.52% is obtained. In the experimental procedure, a 15-gauge needle with an outer diameter of 1.835 mm fixed to a syringe mounted on the device is used to take the test fluid within its container and to produce droplets with a controlled flow rate and volume [15].

Once the droplet is produced, it is deposited on the substrate and the instrument records and digitally analyses its shape. A baseline is then adjusted on the contact line of the substrate. The reported CA values are measured within a few seconds following the deposition. They represent the mean of left and right contact angle. Two methods which are part of the analysis software are considered for CA evaluation: Young-Laplace equation and ellipse method.

2.3.4 Goniometer Surftens Universal (IK4)

Contact angle measurements at IK4 are carried out employing a Surftens Universal Goniometer (ASTRONICS Technologies Pte. Ltd., Singapore). The goniometer consists of an automatic liquid dispenser for dosing controlled droplet volumes and a mobile platform to deposit the substrate. The latter component allows for adjustments of the distance between the syringe carrying the test liquid and the stainless steel substrate. A camera focusses on the droplet and records digital images which are then processed by an integrated software. Contact angle is predicted based on the Young-Laplace equation. The goniometer has a measuring range from 1 to 180° with a resolution of ±0.05°.

The experimental protocol employed is performed under controlled temperature and humidity conditions. It contains the following steps:

1. Before and after each measurement, the substrate is cleaned by sonication for 60 s; for that it is immersed in a glass with DI-water and then dried with a microfiber tissue.
2. A drop of controlled volume is deposited on the substrate, and the CA is measured at 0 s and 10 s.

In the sequence of tests, the DI-water is measured first, followed by the proposed nanofluids.

2.3.5 Goniometer DSA100 (Krüss) Drop shape analyser (UoL)

For each measurement, a droplet is dosed by a needle (Krüss GmbH, Germany) onto the substrate. It takes about 10 s for light focusing, and another 10 s to measure the contact angle. For each single contact angle value, the time duration is about 30 sec. All measurements are performed at a similar time scale, i.e. tens of seconds. For each fluid, the contact angles are measured five times. An average value is calculated based on three intermediate values, excluding the maximum and the minimum value.

During the tests, the central position is first checked by adjusting the x-y-z supports, without contact angle measurements, including both positioning of the stainless steel substrate and positioning of the droplet on it. Before each measurement, the substrate is sonicated for 9 to 10 min in tap water, then rinsed with ethanol, and then with milli-Q water three times. After that, the plate is gently dried with a nitrogen gas gun.

First, measurements are carried out for DI-water, and then the nanofluids are measured.

2.3.6 NAITEC device (NAITEC)

The set-up used by NAITEC (Fig. 3) for the contact angle measurements consists of three main components:

1. a flat platform for the stainless steel substrate to test and adjust the height,
2. an electronic micropipette to dose a fixed droplet volume, and
3. a digital camera to register the images.

These images are subsequently used to determine CA employing ImageJ, a free software. The procedure for the contact angle measurement is as follows:

1. Adjust the height between platform and end of the micropipette.
2. Adjust the dispense speed and the drop volume of the micropipette.
3. Place the substrate on the platform.
4. Dose one droplet on the substrate and take a digital image.
5. Repeat step (4) six times on different sites of the substrate to check the surface homogeneity.
6. Process the images with the software to obtain contact angles.
7. Final contact angle is the mean of the six measurements.

2.3.7 ILK device (ILK)

The ILK device for determining CA is an in-house built apparatus (Fig. 3). Main components are a sample table carrying the stainless steel substrate, an indirect light source with 129 LEDs (WALSER GmbH & Co. KG, Germany), a light disperser, and a digital reflex camera (Canon EOS 40D). The camera is equipped with a close-up lens (Tamron, SP 90 mm F/2.8, Di MACRO 1:1, VC USD; Japan). A pipette (VWR Pipettor 2-20 μl) is utilised to position the droplets on the substrate. A precision thermometer (Greisinger GMH3710, GHM Messtechnik GmbH; Germany) is employed to measure the temperature directly above the droplet.

The camera is connected with a laptop to store and process the droplet images. Determination of contact angle is carried out employing ImageJ, including extension “drop analysis” [16]. The contact angle of each analysed droplet is determined on both sides. Six droplets are analysed to calculate mean and variance. Time span between droplet position and taking the photo to determine the contact angle ranges between 10 and 20 sec.

2.3.8 UoP device (UoP)

The UoP device is designed to measure the contact angle of fluids at ambient condition. A High Speed Video Camera (Phantom v9.1) equipped with a NIKON 200 mm macro lens and a Nikon 1.7x teleconverter is positioned in front of the stage where the droplet is located. The droplets are deposited on the surface of the stainless steel substrate by means of a calibrated 50 μL Hamilton syringe equipped PB600-1 dispenser and illuminated from the back by a single LED cold source.

After a sensitivity analysis, 5 μl is selected as reference volume for the contact angle measurements. This avoids the pooling effect and minimises the volume uncertainty, which is estimated to be around ±0.5 μL. The droplet shape analysis is conducted using a free referenced plugin software for ImageJ called ‘‘DropSnake” [17].

Contact angles are measured on the basis of 6 independent droplets randomly deposited on the surface of the substrate. From the recorded video of each droplet, 3 frames are extracted and analysed. In the end, 18 frames for each fluid are investigated. Contact angles on both sides of the droplets are determined. The first value of the given contact angle of each fluid is therewith the average of 36 measurements. Finally, the average value excluding the highest and the lowest CA data points is calculated and presented in this study.

2.3.9 Biolin Scientific – Attension Tensiometer (UoB)

UoB employing the Wilhelmy plate method carried out additional experiments with respect to the dynamic contact angle. This method is based on the load measurement during

interaction of a thin plate with the free surface of a liquid. For the measurements a thin plate of 10 mm wide, 20 mm length, and 0.8 mm thickness, consisting of the same material as all other solid substrates is employed.

When the stainless steel plate submerges into the liquid, the advancing contact angle θ_{ad} is determined. The receding contact angle θ_{re} is obtained when the plate is pulled out of the liquid. A computer-controlled Sigma 700 force tensiometer (Biolin Scientific, Sweden/Finland) is employed to measure the loads. The tensiometer has an auto-calibrating microbalance that is capable of measuring loads up to 210 g with a resolution of ±0.01 mg. It performs measurements in a range of 1 mN/m to 2000 mN/m with a resolution of 0.001 mN/m.

In the first stage, surface tension γ of each sample is measured using the du Noüy method as described in [39] at a temperature of 20 °C. The values of the surface tension are used later on to determine the dynamic contact angles using the Wilhelmy plate procedure. In order to establish the precision of the measurements, surface tension of distilled water is measured in a temperature range between 20 °C and 50 °C and compared with the values provided by NIST [29], are compiled in Table A4 of the Supplementary Material. For all measurements performed, the maximum deviation is 0.5%. Based on values of forces per length (*F/l*) during advanced and receding stages, which are within the range of *F/l* = (-7.00, 60.00) mN/m, the maximum deviation of the measured angle, θ = ArcCos [(*F* / *L*)/ γ], is $\Delta\theta_{max}$ = 0.4°.

2.4 Thermophysical properties of nanofluids

Densities ρ of the nanofluids are measured by USdC employing a DSA-5000 equipment (Anton Paar, Austria), whose core part is a U-shaped glass vibrating-tube densimeter. The temperature is controlled within ± 0.005 K by a built-in thermostat. The apparatus is calibrated with ultrapure water (Elix 3 purification system, Millipore Corporation, USA) and dry air. The standard uncertainty of density measurements is estimated to be $5 \cdot 10^{-6}$ g·cm^{-3}.

Thermal conductivity is measured by DEU using a lab made setup which uses an hot-wire thermal probe with AC excitation and 3ω lock-in detection [21]. The thermal probe is made of a nickel wire which has a length of 19.0 mm and a diameter of 40 μm. The probe is used both as thermometer and heater. Application of sinusoidal alternating current at a frequency of ω results in generation of a heat source and temperature fluctuations at 2ω depending on the thermal characteristics of the wire and the surrounding medium. Also, the heater resistance is disturbed by these temperature fluctuations at 2ω and results in a voltage signal at 3ω. In order to determinate thermal conductivity, the amplitude and the phase of the 3ω voltage signal is detected and substituted into a mathematical model. The 3ω voltage signal is measured by using a lock-in amplifier with third-harmonic detection and separated from 1ω

to achieve good signal-to-noise ratio by using a Wheatstone bridge. The measurements are performed at 22 °C and at frequencies of 0.5 Hz, 1 Hz, and 2 Hz. For validation of the setup, thermal conductivities of pure fluids, i.e. DI-water and ethylene glycol, are measured and *k*-ratios k_{exp} / $k_{reference}$ are found within an accuracy of ± 2 %. For the case of repeated measurements of nanofluid samples considered in this study, repeatability of *k*-ratios is found within ± 0.3 %. All nanofluids are measured three times. Before and after each measurement, the thermal conductivity of pure water is measured for equipment validation.
Shear flow behaviour and viscosity of nanofluids are experimentally evaluated by UR1 employing a Malvern Kinexus Pro stress-controlled rheometer (Malvern Instruments Ltd©, United Kingdom) equipped with a cone-and-plate geometry. The angle and diameter of the cone are 60 mm and 1º, respectively. The device is suitable for low viscous dispersions. Measurements are performed at 21°C and under steady-state conditions imposing a logarithmic shear stress ramp. The latter was selected to cover a shear rate range between 10 and 1.000 1/s for each nanofluid sample. The temperature is established and controlled by a Peltier temperature control system with a precision of ± 0.1°C. Measurements are done after a holding time of 300 s to allow the sample to adjust to the surrounding temperature. The sophisticated experimental procedure applied is described detailed in [22], where the uncertainty in viscosity measurement is reported to be less than 4 %.

3. Results and discussions

The following sections discuss the thermophysical properties and give an overview on the obtained contact angle data and their analysis. Table 1 compile the colour code for all data presentations. The nomenclature provides abbreviations for all institutions involved in the measurements of this study. Data are represented with always the same symbol throughout all graphical representations. Dots stand for the reference fluid DI-water and squares for the NaCl-solution. Graphene oxide nanofluid is represented by upright triangles, alumina nanofluid by diamonds and the gold nanofluid by stars.

3.1 Thermophysical properties

Thermophysical properties – density, viscosity, and thermal conductivity – are compiled in Fig. 4. Density of gold and graphene oxide nanofluids coincide nearly perfectly with the equivalent values of DI-water [29]. The reason for the marginal departure (less than 0.1 ‰) is either the low concentration (Au NF) or the low density of the nanoparticle material (GO NF). It is assumed that the apparent density of graphene oxide sheets is close to that of graphite and ranges between 1.5 and 1.9 g/cm³ [30]. The alumina nanofluid has a slightly higher

density than DI-water. At 20 °C the increase amounts to 0.26 %. However, the temperature dependency of this nanofluid also reflects that of DI-water.

The middle plot of Fig. 4 depicts the viscosity of the three nanofluids. Due to its extraordinarily low concentration and no addition of any surfactant, the gold nanofluid shows a Newtonian behaviour which is nearly identical to DI-water. The alumina nanofluid behaves weakly and the graphene oxide nanofluid moderately non-Newtonian. Both suspensions are shear thinning. Plotted in a log-log diagram, data for both nanofluids depict linear correlations between dynamic viscosity and shear rate, which points in both cases toward a power law characteristic. Amplitude and extension with shear rate of shear-thinning region is more pronounced with the graphene oxide than for the alumina nanofluid. Viscosity of the alumina suspension at high shear rate tends towards that of DI-water while it is higher for the graphene oxide nanofluid.

Thermal conductivity of graphene oxide and alumina nanofluids (lower plot of Fig. 4) is about 0.4 % below that of DI-water. The gold nanofluid shows nearly the value of DI-water. The influence of nanoparticles on the thermal conductivity of the suspensions is therewith negligible.

To summarise, the gold nanofluid behaves, with respect to density, viscosity, and thermal conductivity, more or less like DI-water. For the alumina nanofluid, only weak departures from the DI-water parameters are found. Concentration is higher here, but still low enough not to induce significant effects. The graphene oxide nanofluid behaves similarly with respect to density and thermal conductivity. However, its viscosity is clearly non-Newtonian.

3.2 Contact angle – Effect of stainless steel substrate

Because each team has only one substrate available, cleaning is a challenging task. This is especially true when it comes to nanofluids. The goal here is to completely remove all remaining nanoparticles after each measurement.

Schuster et al. [12] find on a stainless steel surface that no cleaning leads to increasing contact angles with consecutive droplets. On the other hand, these authors report that cleaning with acetone or ethanol does not affect measured contact angle values. Preliminary experiments carried out at NAITEC revealed that if isopropyl alcohol is used for cleaning the substrate's surface, a reduction of the CA of up to 10° is observed. The fact that cleaning strategy employing acetone or even DI-water may affect CA measurements is confirmed by additional experiments at ILK. It seems plausible that any liquid remainder of the detergent, or also a surface coating which may follow from dried detergent, affects the contact angle. In general, any wetness on the surface undermines the intension to measure advancing contact angles, which are characterised by the *initial formation of wetting lamella* due to adhesion of

the liquids to the solid surfaces, which is a soft substrate [26]. Therefore, after any cleaning a strict drying is needed.

Trials which make use of ultra-sonication of the surface of the substrate indicate an influence on surface roughness and therewith on the measured CA values [27]. The general finding of this specific tests carried out with one of the substrates is that R_a remains constant while R_z decreases (see Table A2 of Supplementary Material). Roughness is measured employing a Profilometer DEKTAK 8 (FILMETRICS, Inc., USA).

The fact that ultra-sonication might affect metallic surfaces by cavitational erosion is known [28]. In contrast, immersing the substrate in water kept in a beaker which is then placed in a standard ultrasonic cleaner for cleaning seems to be an acceptable strategy (UoL). The polished face of the substrate should be in contact with water, but not touch the beaker wall. NAITEC carried out experiments without and with such an indirect ultra-sonicating and found no differences in the measured contact angles. Similarly, IKCU found that ultra-sonication is a proper cleaning strategy.

To summarise, ultra-sonication seems to be an adequate procedure for removing nanoparticles from stainless steel substrates in preparation for consecutive tests. However, it is most important that results of several independent experiments are compared to check if cleaning affects experiments. This strategy is applied here. All data are seen in context. Moreover, careful inspections of substrate surface and reference measurements are needed to exclude any flaws following from inappropriate cleaning.

According to point (5) of the NAITEC procedure (Sec. 2.3.6), contact angle measurement is carried out at six different positions of the substrate to check its homogeneity. The mean CA value obtained for DI-water (t = 23.0 °C, V_{dr} = 19 μl) is 68.7° with a standard deviation of 1.78°. Similar for graphene oxide and alumina nanofluid at the same temperature and with the same droplet volume, standard variances of 1.75° and 1.34°, respectively, are found. UoP has a similar strategy (Sec. 2.3.8) measuring at six positions and averaging over 30 data points. The standard deviations found at UoP for DI-water are 1.93°, for GO nanofluid 1.31°, for alumina nanofluid 1.31°, and for gold nanofluid 2.21°. These two independent results indicate that position of the droplet on the substrate has only a weak influence on contact angle compared to temperature and droplet volume.

3.3 Contact angle – Raw data

For illustration, photos of droplets of all four liquids – UJI in-house built device – are shown in Fig. 5. Contact angle raw data in dependency of temperature as they are provided by the participants of the round robin test are compiled in Fig. 6. Some of the participants delivered data taken with different droplet volumes, but at constant temperature. These data sets form

columns in the diagrams. Note that all data are represented with error bars indicating the variance of the obtained values. However, in the most cases these error bars disappear in the symbols.

The first diagram shows, beside the DI-water data, also one result for the base fluid of the gold nanofluid. As discussed in Sec. 2.1.3, this suspension is stabilised with 0.1 mmol/l NaCl. Therefore, one of the teams (NAITEC) carried out a measurement employing a NaCl-solution with the same concentration. The results taken at the same temperature utilising the same droplet volume – DI-water: 68.7°, NaCl-solution: 71.5°, gold nanofluid 67.9° – indicate that the difference is small and well within the scatter of data. That the influence of a NaCl concentration of 0.1 mmol/l in water is actually negligible is shown in [31].

Data analysis of the Wilhelmy method (UoB) revealed that the CA results are influenced by the state of the surface – dry or wet – of the UoB sample. The procedures employed, either optical or using a force tensiometer, indicate different values for θ_{ad} by either submerging a dry or a wet surface of the stainless steel sample into the test liquids. This effect is known as the initial formation of wetting lamella [26]. For determining θ_{re} there is no other option then to pull out an already wet sample. Usually the static contact angles is determined as the mean of advancing and receding angle or the arc cosine of the mean of the cosines of the two angles [2]. Plots of Fig. 6 show the advancing and, hence, dry surface condition during the first measurement of each cycle, and the receding and, hence, wet surface condition contact angles and the two static CA following from these data.

The stability over time of nanofluid samples is investigated by two experimental series carried out on Feb. 21st and on March 9th, 2018, employing a Krüss Goniometer DSA100 Drop shape analyser (UoL). Both experimental series are conducted at the same temperature, 22.1 °C, and with the same droplet volume, 2 µl. The results of both runs indicate with 72.8°, 71.7° (DI-water, -1.53 %); 63.7°, 66.7° (GO nanofluid, +4.50 %); 83.5°, 82.8° (alumina nanofluid, -0.84 %); and 82.6°, 82.6° (gold nanofluid 0 %) reasonable agreement. Observation with the naked eye (ILK) of gold and graphene nanofluid stored in glass ampullas (Fig. 1) indicates no visible sedimentation for several weeks. Weak sedimentation is observed for the alumina nanofluid, which could be removed by sonication or even by intense shaking.

The measurement device (DSA-30 Drop Shape Analyzer) employed by UR1 allows different methods to determine the contact angle value. Within this study, both the well-known Young-Laplace equation and the ellipse method are considered for all investigated fluids. The latter approach simply consists of fitting an ellipse in the evaluation of the sessile drop outline. No significant differences between both methods are found for any of the investigated fluids.

In general, all four analysed liquids show a tendency for lowering the contact angle with increasing temperature (Fig. 6). This effect seems to be stronger for the three nanofluids

compared to DI-water. The observable scatter follows not simply from experimental error, but rather from the different droplet sizes utilised (see Table A3 of Supplementary Material). To cope with this complexity, a strategy is proposed in the following section.

3.4 Contact Angle – Data Processing

Based on the theoretical consideration – density and surface tension being two temperature and pressure dependent thermophysical properties which affect droplet contour [11] – it is argued that a measured contact angle depends on the local temperature. Note that local temperature does not simply mean any sort of ambient temperature, but rather the temperature of the thermal field actually affecting the contact angle.

Therewith, contact angle measurements are a non-isothermal task. Meaning it is the mass of the nanofluid utilised for the measurements and not its volume that matters. Based on this fact and on the theoretical considerations by Vafaei and Podowski [11], who showed that the contour of a droplet depends on its weight, it is argued that the contact angle of a droplet correlates with its mass. If the experimental temperature is fixed or changes only slightly, this correlation can be replaced by a dependency of the droplet volume. The existence of such correlations for DI-water on stainless steel has been experimentally confirmed [12].

The shape of an experimentally investigated sessile droplet depends on external fields such as gravity, electrical or magnetic field, etc. [40]. Under these circumstances a single-phase droplet is not spherical, despite the fact that it might be axisymmetric [11]. It should be mentioned that droplets with a characteristic length scale less than the capillary length, which is about 2.7 mm for pure water, show a spherical shape even under terrestrial conditions [41]. Experimental studies [13] indicate that decreasing the volume of a single-phase droplet drives the contact angle asymptotically to a constant value at zero-volume. However, it seems to be an open issue, if this dependency is appreciable [12, 13] or rather weak [42,43]. Consequently, the contact angle under zero-volume condition is a function of temperature and pressure, as with any other thermophysical property. It is assumed that this conclusion is, to the first order, also true for two-phase nanofluid droplets.

Combining the above arguments, the contact angle is describable by a Taylor series expansion of two variables: local temperature and droplet volume. The droplet volume V_{dr} stands for the characteristic geometrical length of the droplet l_{dr} which is the cube root of this parameter. The Taylor series – truncated to the first order term – reads then

$$\theta_{fl}\,(t, V_{dr}) = a_{0,fl} + a_{t,fl}\,t + a_{V,fl}\,l_{dr}, \qquad l_{dr} = V_{dr}^{(1/3)} \tag{1}$$

where θ_{fl} (t, V_{dr}) denotes the contact angle of a certain fluid at a given temperature *t* for a certain droplet volume V_{dr}.

The last term of eq. (1) should not be confused with a representation of line tension. Line tension and reactive wetting are represented by additional terms in Young's equation [44]. That the line tension term then is mostly written in the form $\Gamma / (r_{dr}\ \gamma_{lv})$ does not necessarily lead to the interpretation that the limiting contact angle becomes ill defined. Molecular dynamical results [45] rather indicate, that Γ varies with droplet size and contact angle approaches at sufficiently small droplet radii a saturation of $cos(\theta) = 1$. However, eq. (1) is not about these effects. It rather summarises any influence related to temperature and volume affecting the contact angle based on heuristic assumptions.

From an experimental point of view it is impossible to create droplets of zero-volume. Moreover, droplets with very small volume may increase experimental error significantly. Therefore, based on the above considerations, it is proposed to employ the limiting value of eq. (1) for zero-volume $\theta_{fl,0}\ (t, 0)$ as the characteristic contact angle of a nanofluid. To obtain this limiting value, a sufficient number of data points with finite droplet volume have to be fitted employing eq. (1) to determine the coefficients $a_{0,fl}$, $a_{t,fl}$, and $a_{V,fl}$. By taking the limit for $V_{dr} \rightarrow 0$, a linear function for θ_0 is found. The pressure dependency of the limiting contact angle is excluded due to the weak compressibility of water under ambient conditions.

The proposed data processing consists of three steps:

1. Fitting of the data according to eq. (1).
2. Determining the limiting contact angle for zero-volume
$$\theta_{fl,0} = \theta_{fl}\ (t, 0).$$
3. Analysing the temperature dependency of $\theta_{fl,0}$.

Fitting is carried out by employing the Levenberg–Marquardt algorithm [32] implemented in MATHEMATICA 10.2. The obtained coefficients $a_{0,fl}$, $a_{t,fl}$, and $a_{v,fl}$ are compiled in Table A5 of the Supplementary Material. The data obtained with the Wilhelmy plate method (UoB) are not considered in the fitting procedure because they provide other parameters than the sessile drop methods.

Experimental data analysed here range between 19 °C and 25 °C. The density of DI-water at these temperatures amounts to 998.55 kg/m^3 and 997.25 kg/m^3 (NIST data base [29]), respectively, which correlates to a lowering of 1.3 ‰ over the considered temperature range. This fact and the marginal differences between the density of DI-water and the densities of the nanofluids allow the application of eq. (1). It is sufficient to consider droplet volume instead of droplet mass as a parameter.

In the first step, the DI-water data are approximated. The first diagram of Fig. 7 shows that the experimental data (horizontal axis) and the predicted data (vertical axis) based on θ_{H2O} *(t,* V_{dr}*)* are in reasonable agreement. The majority of the data is found in the error band of ±10 %. To confirm the found dependency, data from several independent references [5,33–35] are utilised. Because temperature, droplet size, and experimentally obtained contact angle are given in these publications the contact angle according to eq. (1) could be predicted and depicted in Fig. 7.

Most of the reference data are found in the error band of ± 10 %. Zhao et al. (2004) [26] employed with EN 1.4301°, AISI/ASTM 304 the same steel grade as this study. However, only data which are in the temperature range investigated here are considered from Zhao's study. All experiments by Kim et al. (2007) [5] including nanofluids are carried out on EN 1.4401°, AISI/ASTM 316. Experiment by Orazi et al. (2015) [34] are carried out on AISI 316 L. Prajitno et al. (2016) [35] use stainless steel AISI/ASTM 304 grinded with different grit emery paper. First plot of Fig. 7 shows data for the grits 500, 800, and 1000.

The second and third diagram of Fig. 7 are quality checks for the graphene oxide and the alumina nanofluid. In both cases the scatter is slightly larger than for DI-water. The alumina results are confirmed by an independent data point from [5]. For the gold nanofluid the data are again found within the ± 10 % error band.

The last quality check plot compiles all data including DI-water. For each liquid the corresponding fitting function is applied. The majority of the data is within the ±10 % error band, which confirms the validity of the proposed fitting strategy.

Figure 8 depicts the fitting function for DI-water in dependency on the droplet volume for the three temperatures 19, 22, and 25 °C. These three temperatures resemble the range spanned by the experiments (see Table A3 of Supplementary Material). Due to the weak dependency on temperature, the curves appear as if they have just been shifted along the vertical axis. At zero droplet volume the curves indicate $\theta_{H2O,0}$*(t,* V_{dr} *= 0)* the contact angle under for zero-volume condition.

For comparison, the contact angle correlation [12] for DI-water on stainless steel (EN 1.4401°, AISI/ASTM 316) is plotted. This correlation gives about 20° lower contact angles, which might be due to different roughness and/or chemical composition of the substrate. However, the inclination of Schuster's correlation and therewith the dependency on the droplet volume is comparable with the curves proposed here. To illustrate this, Schuster's correlation is shifted and extended so that it matches the fitting curves for 19, 22, and 25 °C at a droplet volume of 8 µl (coloured broken lines).

With Fig. 8 the fitting function of DI-water θ_{H2O} *(t,* V_{dr}*)* and the equivalent correlations for the nanofluids are compared at 22 °C for illustrative purposes. Additionally, the experimental data are re-plotted. For that purpose the actual droplet volumes are inserted in the fitting

functions. Temperature is chosen in all cases as 22 °C. Symbols in Fig. 8 render therewith the experimental data as if they had been taken at this temperature. Removing the temperature dependency indicates

1. how actually similar the contact angles of DI-water and the alumina and the gold nanofluid are,
2. that the dependency of the contact angle on the droplet volume of DI-water, alumina, and gold nanofluid are nearly identical, and
3. the much stronger and different dependency of the contact angle of the graphene oxide nanofluid on the droplet volume compared to DI-water.

To emphasise these three findings, ±10 % bands (broken curves) with respect to the fitting functions are plotted. The ±10 % bands are chosen because they render the region where the most experimental data are found (Fig. 7).

With respect to the outcomes following from Fig. 8, it is emphasised that all three nanofluids have low nanoparticle concentrations. Moreover, only the gold nanofluid is mildly stabilised with a dissociating prototypical salt. Any change of the contact angle compared to pure DI-water may therefore be attributed to the nanoparticles. Hence, it is not surprising that the alumina and the gold nanofluid – both with rigid spherical nanoparticles – behave similarly. The situation is different for the graphene oxide particles. These *fluffy* nano-objects have an extraordinarily large length / width to thickness ratio (Sec. 2.1.1) and may consequently affect the surface tension and, therewith, the contact line and angle differently. This finding is similar to the changes of the dynamic viscosity, which is strongest for the GO nanofluid.

In Fig. 9 the limiting contact angle for zero-volume is depicted graphically. Table A6 of the Supplementary Material gives for 19, 22, and 25 °C the limiting contact angles for DI-water and the three nanofluids. The limiting contact angle $\theta_{fl,0}$ is basically the searched thermophysical property, depending on the temperature, the surface energy of the substrate, the solid-liquid interfacial interaction and the specification of the nanofluid. Due to the first order approximation of the temperature dependency in eq. (1), the shown correlations appear linear (Fig. 9). At first glance it appears that all lines have a negative inclination, which is stronger for the nanofluids than for DI-water. The general trend of DI-water – the higher the temperature the less $\theta_{H2O,0}$ – is therewith preserved for all nanofluids. That seems to be plausible because the overwhelming component of all suspensions is DI-water. Hence, the found differences between nanofluids and DI-water and between the nanofluids can be attributed more or less to the nanoparticles solely. A possible explanation for the different

inclinations (meaning different dependencies on the temperature) may follow from the argument that the effective surface tension of the different nanofluids is differently affected by temperature.

As a side note it should be mentioned that a special behaviour of the dynamic contact angle is noticed for GO nanofluid (UoB-measurements). When the surface becomes wet, after the first measurement during the testing cycle, the advancing contact angle value goes down to zero $\theta_{ad} \rightarrow 0$, revealing a situation when the liquid stretches over the surface. This wetting hysteresis indicates a possible interaction between graphene oxide particles and solid substrate and therewith an interaction between measurement device and nanofluid. It has to be mentioned that similar effects are not observed for sessile droplets of all nanofluids investigated.

4 Strategy for determining the contact angle of nanofluids

Only the contact angle for zero-volume, can be understood as a characteristic material property of a nanofluids droplet placed on a certain solid substrate under a certain atmosphere. To cope with this fact and to find this property, the following strategy is proposed.

a) Both base fluid and nanofluid have to be investigated to quantify the influence of the nanoparticles on the contact angle of nanofluids. Note that the de facto base fluid may consist of the pure base fluid and some chemical cocktail employed to stabilise the suspension against agglomeration. Moreover, it should be proved that the substrate is sufficiently homogeneous.
b) A sufficient number of contact angle measurements under varying temperatures and with different droplet volumes for both base fluid and nanofluid have to be carried out. If the substrate is not renewed from experiment to experiment, a proper cleaning strategy must be chosen to remove remaining nanoparticles. Ultra-sonication seems to be such a procedure in preparation for consecutive tests.
c) Fitting of experimental data employing a physically founded approach delivers correlations depending on temperature and droplet volume.
d) Only the comparison of the limiting contact angles of base fluid $\theta_{H2O,0}(t, V_{dr} = 0)$ and nanofluid $\theta_{nf,0}(t, V_{dr} = 0)$ provides information on the characteristic differences between base fluid and nanofluid.

5 Conclusion

For the first time the contact angle of dilute water based nanofluid droplets placed on a stainless steel substrate was measured within the frame work of a round robin test. Nine European research laboratories determined the contact angle of graphene oxide, alumina and gold nanofluids. Based on the results it is demonstrated, that the contact angle for zero-volume $\theta_{fl,0}(t, 0)$ can be predicted from a sufficiently large data base of contact angles. The round robin test indicates, that the contact angle of sessile droplets of dilute nanofluids can be measured exactly without influences from the measurement technique. However, cleaning strategy may have a strong influence and must be chosen carefully. All remainders of detergent and any nanoparticles remaining from previous tests on the sample have to be removed thoroughly.

Differently to most other contact angle studies on nanofluids [see e.g. 36-38] the contact angle for zero-volume $\theta_{fl,0}$ is considered as the proper thermophysical property to characterise dilute nanofluids. This limiting contact angle depends on the temperature, the surface energy of the substrate, the solid-liquid interfacial interaction and the specification of the nanofluid. The general trend found for deionised water – the higher the temperature the less $\theta_{fl,0}$ – is preserved for all nanofluids which indicates, that the found differences between the different fluids are caused by the nanoparticles.

Further research is underway with respect to surface tension of dilute nanofluids [14]. Both contact angle for zero-volume and surface tension will be the basis for proper modelling of nanofluid heat transfer with phase change taking place on a certain surface under a certain atmosphere.

Acknowledgement

This article is based upon work from COST Action CA15119 NANOUPTAKE, supported by COST (European Cooperation in Science and Technology).

The authors would like to acknowledge the efforts of the many people behind the scenes – students, technicians, laboratory assistants, postal workers, etc. – involved in the project.

KGS and MHB gratefully acknowledge support from the Bundesministerium für Wirtschaft und Energie (Germany) under grant 49VF 170005.

PE acknowledges the European Union through the European Regional Development Fund (ERDF), the Ministry of Higher Education and Research, the French region of Brittany and Rennes Métropole for the financial support of the CA experimental device.

AA acknowledges support from the Spanish Ministry of Economy and Competitiveness and the UE FEDER programme under grants ENE2014-55489-C2-1-R and ENE2017-86425-C2-2-R.

References

[1] COST Action NanoUptake website, (n.d.). http://nanouptake.uji.es/.

[2] C. Tropea, A.L. Yarin, J.F. (Eds. . Foss, Handbook of Experimental Fluid Mechanics, Heidelberg: Springer Verlag, Berlin, 2007.

[3] P. Estellé, D. Cabaleiro, G. Żyła, L. Lugo, S.M.S. Murshed, Current trends in surface tension and wetting behavior of nanofluids, Renew. Sustain. Energy Rev. 94 (2018) 931–944. doi:10.1016/J.RSER.2018.07.006.

[4] S. Vafaei, T. Borca-Tasciuc, M.Z. Podowski, A. Purkayastha, G. Ramanath, P.M. Ajayan, Effect of nanoparticles on sessile droplet contact angle, Nanotechnology. 17 (2006) 2523–2527. doi:10.1088/0957-4484/17/10/014.

[5] S.J. Kim, I.C. Bang, J. Buongiorno, L.W. Hu, Study of pool boiling and critical heat flux enhancement in nanofluids, Bull. Polish Acad. Sci. 55 (2007) 211–216. doi:10.1115/IMECE2007-41697.

[6] J.T. Cieśliński, K.A. Krygier, Sessile droplet contact angle of water-Al2O3, water-TiO2and water-Cu nanofluids, Exp. Therm. Fluid Sci. 59 (2014) 258–263. doi:10.1016/j.expthermflusci.2014.06.004.

[7] J. Chinnam, D.K. Das, R.S. Vajjha, J.R. Satti, Measurements of the surface tension of nanofluids and development of a new correlation, Int. J. Therm. Sci. 98 (2015) 68–80. doi:10.1016/j.ijthermalsci.2015.07.008.

[8] M.H. Buschmann, R. Azizian, T. Kempe, J.E. Juliá, R. Martínez-Cuenca, B. Sundén, Z. Wu, A. Seppälä, T. Ala-Nissila, Correct interpretation of nanofluid convective heat transfer, Int. J. Therm. Sci. 129 (2018) 504–531. doi:10.1016/j.ijthermalsci.2017.11.003.

[9] R.D. Deegan, O. Bakajin, T.F. Dupont, G. Huber, S.R. Nagel, T.A. Witten, Capillary flow as the cause of ring stains from dried liquid drops, Nature. 389 (1997) 827–829. doi:10.1038/39827.

[10] S. Lim, H. Zhang, P. Wu, A. Nikolov, D. Wasan, The dynamic spreading of nanofluids on solid surfaces - Role of the nanofilm structural disjoining pressure, J. Colloid Interface Sci. 470 (2016) 22–30. doi:10.1016/j.jcis.2016.02.044.

[11] S. Vafaei, M.Z. Podowski, Analysis of the relationship between liquid droplet size and contact angle, Adv. Colloid Interface Sci. 113 (2005) 133–146. doi:10.1016/j.cis.2005.03.001.

[12] J.M. Schuster, C.E. Schvezov, M.R. Rosenberger, Influence of Experimental Variables on the Measure of Contact Angle in Metals Using the Sessile Drop Method, Procedia Mater. Sci. 8 (2015) 742–751. doi:10.1016/j.mspro.2015.04.131.

[13] J. Gaydos, A.W. Neumann, The dependence of contact angles on drop size and line tension, J. Colloid Interface Sci. 120 (1987) 76–86.

[14] M.H. Buschmann, NANOTENSION - Round robin test for surface tension and contact angle of nanofluids, in: NanoUptake 4th Work. Groups Meet., Naples, Italy, 2018.

[15] D. Cabaleiro, H. Navas, A. Desforges, Dynamic Viscosity and Surface Tension of Stable Graphene Oxide and Reduced Graphene Oxide Aqueous Nanofluid, J. Nanofluids. 7 (2018) 1–8. doi:10.1166/jon.2018.1539.

[16] ImageJ:Image Processing and Analysis in Java, (n.d.). https://imagej.nih.gov/ij/download/.

[17] A. Stalder, DropSnake and LB-ADSA user manual, 2006.

[18] A. Wlazlak, B. Zajaczkowski, M. Woluntarski, M.H. Buschmann, Influence of graphene oxide nanofluids and surfactant on thermal behaviour of the thermosyphon, J. Therm. Anal. Calorim. 3456789 (2018). doi:10.1007/s10973-018-7632-x.

[19] D. Zhang, B. Gökce, S. Barcikowski, Laser Synthesis and Processing of Colloids: Fundamentals and Applications, Chem. Rev. 117 (2017) 3990–4103. doi:10.1021/acs.chemrev.6b00468.

[20] C. Rehbock, V. Merk, L. Gamrad, R. Streubel, S. Barcikowski, Size control of laser-fabricated surfactant-free gold nanoparticles with highly diluted electrolytes and their subsequent bioconjugation, Phys. Chem. Chem. Phys. 15 (2013) 3057–3067. doi:10.1039/c2cp42641b.

[21] A. Turgut, C. Sauter, M. Chirtoc, J.F. Henry, S. Tavman, I. Tavman, J. Pelzl, AC hot wire measurement of thermophysical properties of nanofluids with 3ω method, Eur. Phys. J. Spec. Top. 153 (2008) 349–352. doi:10.1140/epjst/e2008-00459-7.

[22] S. Halelfadl, P. Estellé, B. Aladag, N. Doner, T. Maré, Viscosity of carbon nanotubes water-based nanofluids: Influence of concentration and temperature, Int. J. Therm. Sci. 71 (2013) 111–117. doi:10.1016/j.ijthermalsci.2013.04.013.

[23] Acciai inossidabili Raccolta di tabelle tecniche, 2018. http://www.centroinox.it/sites/default/files/pubblicazioni/245A.pdf.

[24] Nichtrostender Austenitischer Stahl TK 1.4301, 2006. http://www.thyssenkrupp.at/files/rohre/Werkstoffdatenblaetter/1.4301.pdf.

[25] DIN 4777, Metrology of surfaces; profile filters for electrical contact stylus instruments; phasecorrected filters, 1990-05, original language German, (n.d.).

[26] L. Chen, E. Bonaccurso, T. Gambaryan-Roisman, V. Starov, N. Koursari, Y. Zhao, Static and dynamic wetting of soft substrates, Curr. Opin. Colloid Interface Sci. 36 (2018) 46–57. doi:10.1016/j.cocis.2017.12.001.

[27] M. Hernaiz, NANOTENSION round robin test – Contact angle measurements, in: NanoUptake 4th Work. Groups Meet., Naples, Italy, 2017.

[28] S. Verdan, G. Burato, M. Comet, L. Reinert, H. Fuzellier, Structural changes of metallic surfaces induced by ultrasound, Ultrason. Sonochem. 10 (2003) 291–295. doi:10.1016/S1350-4177(03)00106-8.

[29] NIST Reference Fluid Thermodynamic and Transport Properties Database (REFPROP), (2007). http://www.nist.gov/srd/nist23.cfm.

[30] Properties and characteristics of graphite for industrial applications, 2015.

[31] N. Matubayshi, H. Matsuo, K. Yamamoto, S. Yamaguchi, A. Matuzawa, Thermodynamic Quantities of Surface Formation of Aqueous Electrolyte Solutions: I. Aqueous Solutions of NaCI, MgCI2, and LaCI3, J. Colloid Interface Sci. 209 (1999) 398–402. doi:10.1006/jcis.2001.7890.

[32] P.R. Gill, W. Murray, M.H. Wright, The Levenberg–Maquardt Method, in: Pract. Optim., 1981: p. 136,137.

[33] Q. Zhao, Y. Liu, E.W. Abel, Effect of temperature on the surface free energy of amorphous carbon films, J. Colloid Interface Sci. 280 (2004) 174–183. doi:10.1016/j.jcis.2004.07.004.

[34] L. Orazi, I. Gnilitskyi, I. Pavlov, A.P. Serro, S. Ilday, F.O. Ilday, Nonlinear laser lithography to control surface properties of stainless steel, CIRP Ann. - Manuf. Technol. 64 (2015) 193–196. doi:10.1016/j.cirp.2015.04.038.

[35] D.H. Prajitno, A. Maulana, D.G. Syarif, Effect of Surface Roughness on Contact Angle Measurement of Nanofluid on Surface of Stainless Steel 304 by Sessile Drop Method, J. Phys. Conf. Ser. 739 (2016). doi:10.1088/1742-6596/739/1/012029.

[36] G. Lu, X.D. Wang, Y.Y. Duan, A Critical Review of Dynamic Wetting by Complex Fluids: From Newtonian Fluids to Non-Newtonian Fluids and Nanofluids, Adv. Colloid Interface Sci. 236 (2016) 43–62. doi:10.1016/j.cis.2016.07.004.

[37] D. Wasan, A. Nikolov, K. Kondiparty, The wetting and spreading of nanofluids on solids: Role of the structural disjoining pressure, Curr. Opin. Colloid Interface Sci. 16 (2011) 344–349. doi:10.1016/j.cocis.2011.02.001.

[38] M. Radiom, C. Yang, W.K. Chan, Dynamic contact angle of water-based titanium oxide nanofluid, Nanoscale Res. Lett. 8 (2013) 1–9. doi:10.1186/1556-276X-8-282.

[39] A. Huminic, G. Huminic, C. Fleaca, F. Dumitrache, I. Morjan, Thermal conductivity, viscosity and surface tension of nanofluids based on FeC nanoparticles, Powder Technol. 284 (2015) 78–84. doi:10.1016/j.powtec.2015.06.040.

[40] E. Bormashenko, Contact Angles of Sessile Droplets Deposited on Rough and Flat Surfaces in the Presence of External Fields, Math. Model. Nat. Phenom. 7 (2012) 1–5. doi:10.1051/mmnp/20127401.

[41] A. Diana, M. Castillo, D. Brutin, T. Steinberg, Sessile drop wettability in normal and reduced gravity, Microgravity Sci. Technol. 24 (2012) 195–202. doi:10.1007/s12217-011-9295-0.

[42] R. Tadmor, Line energy, line tension and drop size, Surf. Sci. 602 (2008) 12–15. doi:10.1016/j.susc.2008.05.018.

[43] G. Whyman, E. Bormashenko, Oblate spheroid model for calculation of the shape and contact angles of heavy droplets, J. Colloid Interface Sci. 331 (2009) 174–177. doi:10.1016/j.jcis.2008.11.040.

[44] E. Bormashenko, Apparent contact angles for reactive wetting of smooth, rough, and heterogeneous surfaces calculated from the variational principles, J. Colloid Interface Sci. 537 (2019) 597–603. doi:10.1016/j.jcis.2018.11.068.

[45] J.H. Weijs, A. Marchand, B. Andreotti, D. Lohse, J.H. Snoeijer, Origin of line tension for a Lennard-Jones nanodroplet, Phys. Fluids. 23 (2011). doi:10.1063/1.3546008.

Table 1: Symbol and colour code for data presentation

institution	colour
University of Padova (Italy)	■
IK4-TEKNIKER (Spain)	■
NAITEC (Spain)	■
Lund University (Sweden)	■
Université Rennes 1 (France)	Laplace ■ ellipse ■
İzmir Katip Çelebi University (Turkey)	■
Universitat Jaume I Castelló (Spain)	commercial ■ non-commercial ■
University of Brasov (Romania)	■
ILK Dresden (Germany)	■

Fig. 1: Employed nanofluids. From left to right: GO, Au, and Al_2O_3-nanofluid.

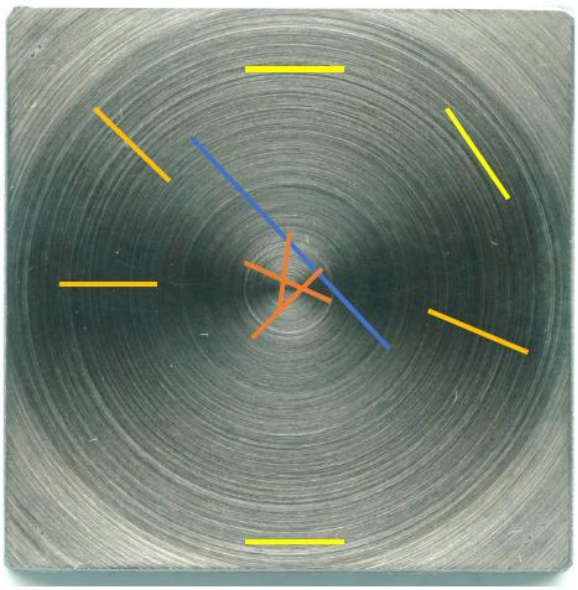

Fig. 2: Frontal view of stainless steel substrate. Droplets for CA measurements are placed right in the centre of the substrate. Lines indicate Perthometer path to measure surface roughness. For measured roughness values, see Table A2 of Supplementary Material.

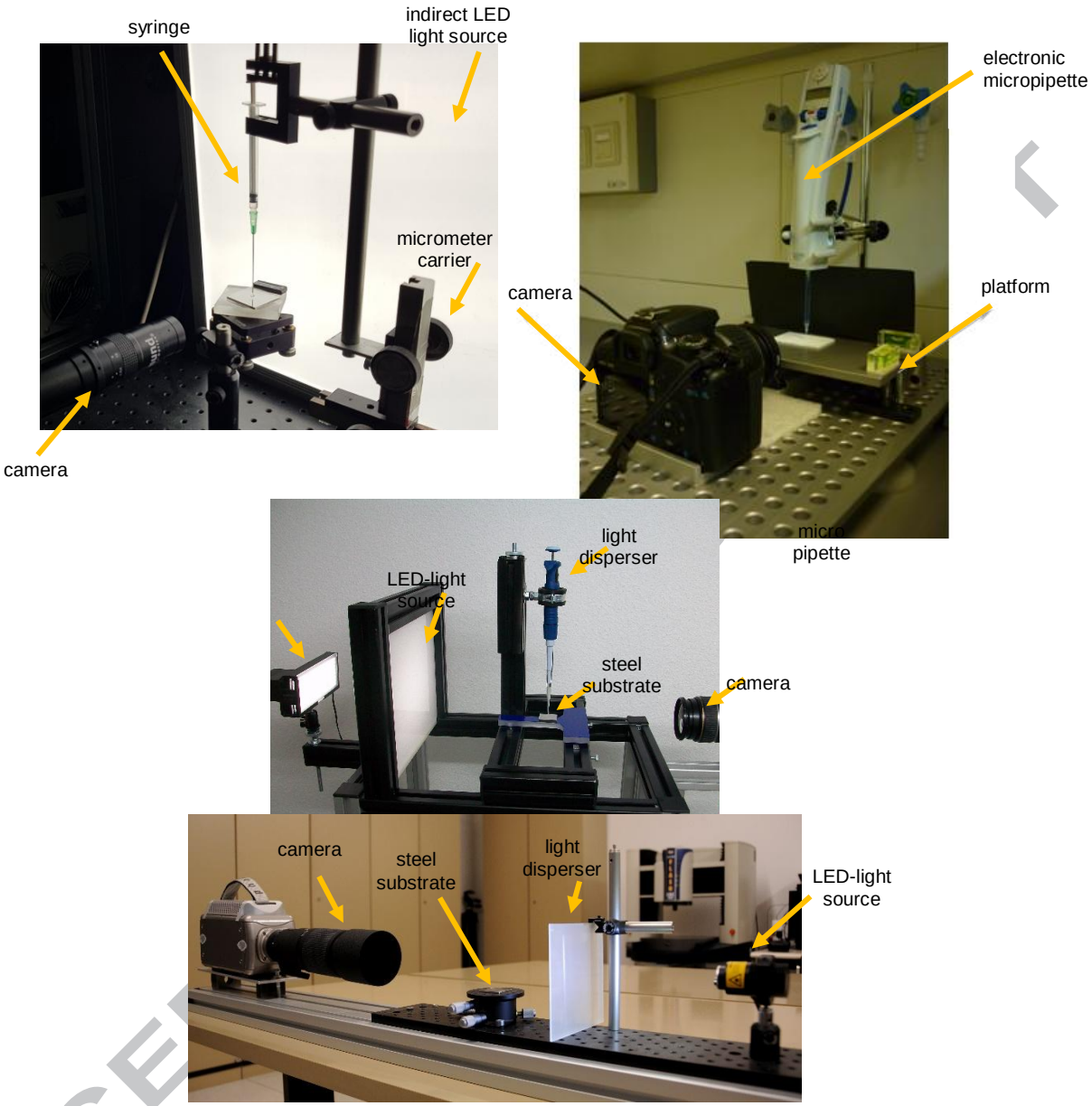

Fig. 3: In-house built contact angle measurement devices. Upper photos show the UJI device (left) and the NAITEC device. Middle photo represents the ILK device and lower photo the UoP device.

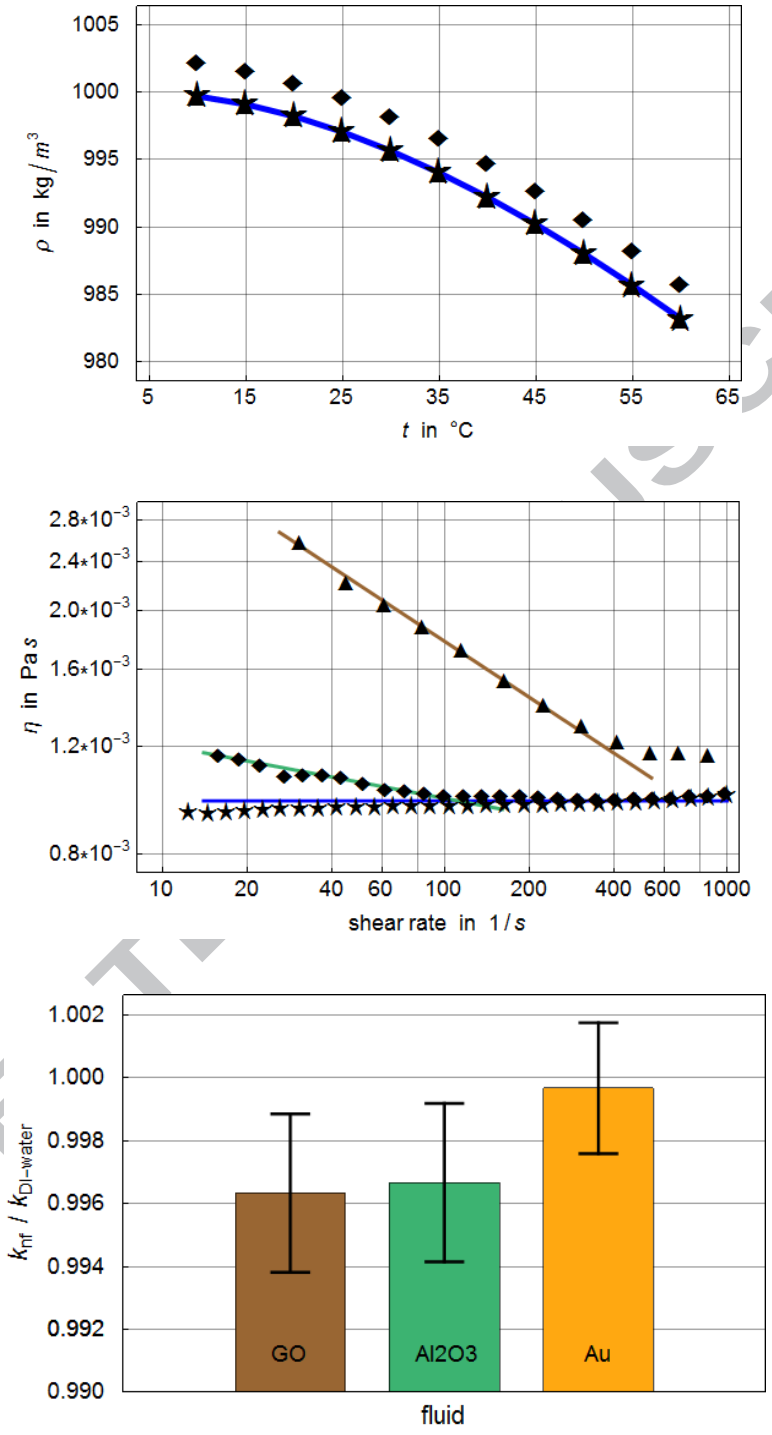

Fig. 4: Characterisation of nanofluids. Upper plot shows density, middle plot viscosity, and bar charts thermal conductivity ratios. Blue line / curve in upper and middle plot indicate water according to NIST database. Brown and green lines show power law fit of GO and alumina viscosity for low shear rates. Error bars in lower plot indicate variance of measurements.

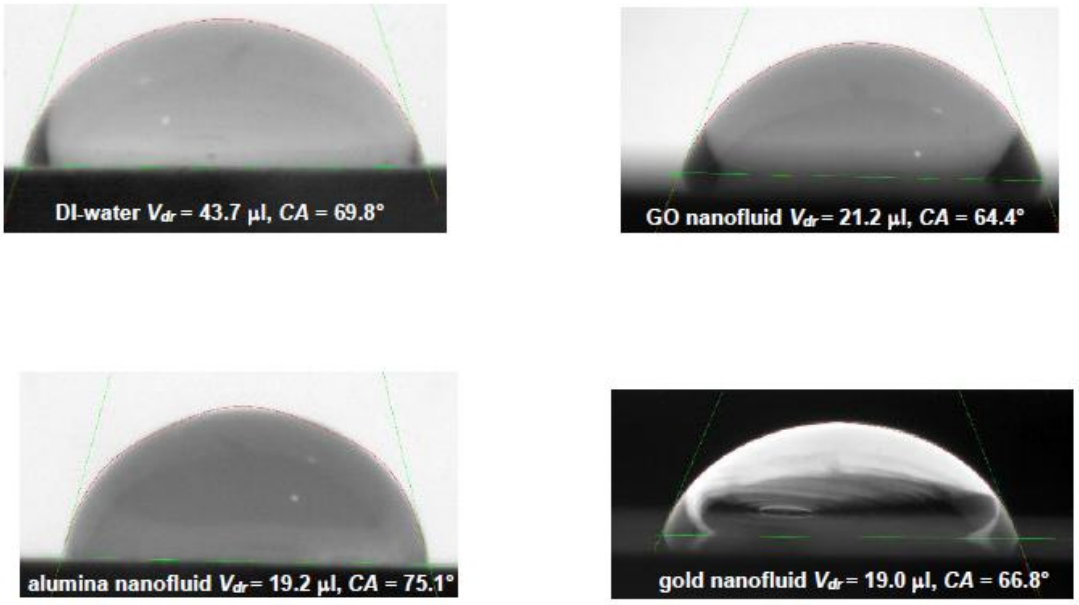

Fig. 5: Examples of droplets for DI-water. GO, gold, and alumina nanofluid (clockwise starting from right top right). Photos from UJI.

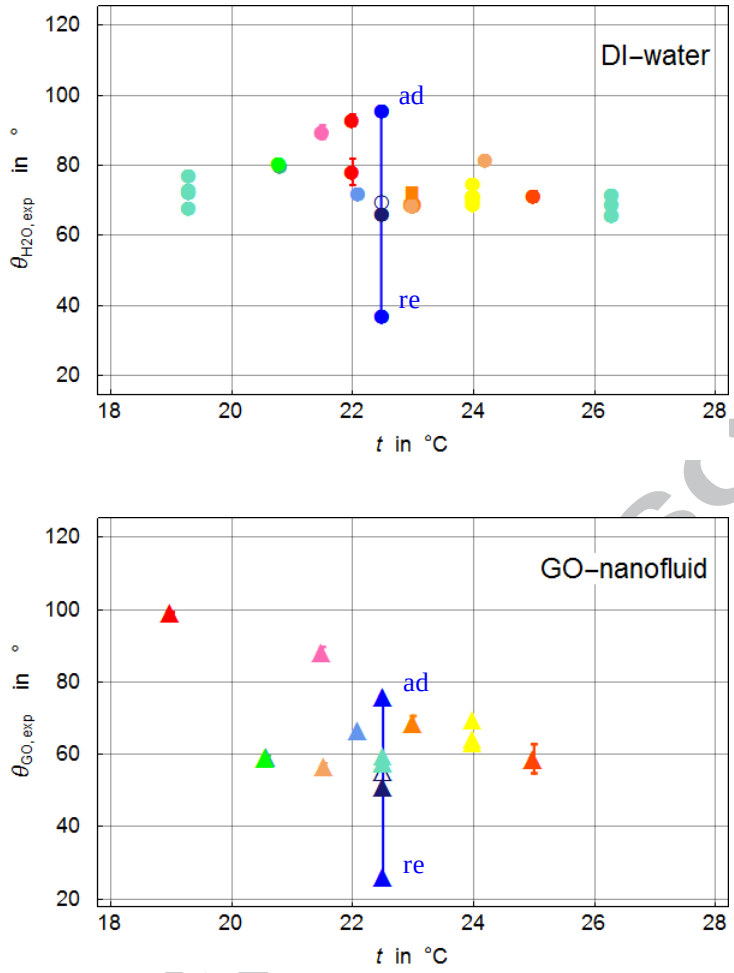

Fig. 6: Raw data of contact angle. Upper plot reference fluid DI-water and lower plot graphene oxide nanofluid. Wilhelmy plate results are connected by vertical lines. The arithmetic mean of advancing and receding CA are depicted by dark blue symbols and the arithmetic mean of their cosines with empty dark blue symbols.

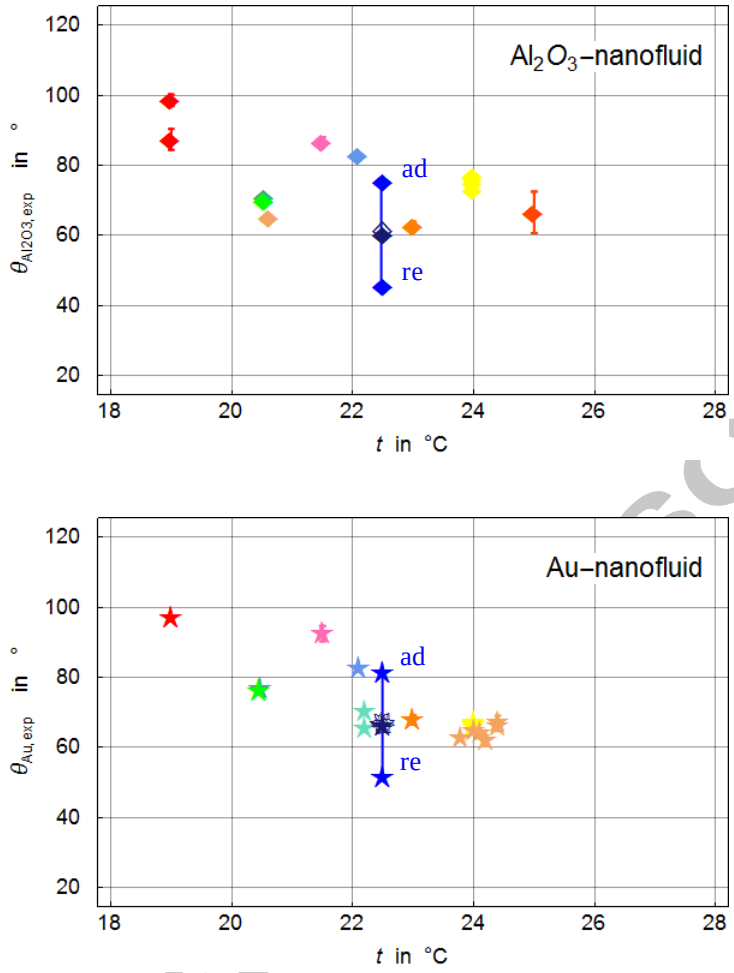

Continuation of previous page

Raw data of contact angle. Upper plot shows alumina nanofluid and lower plot gold nanofluid.

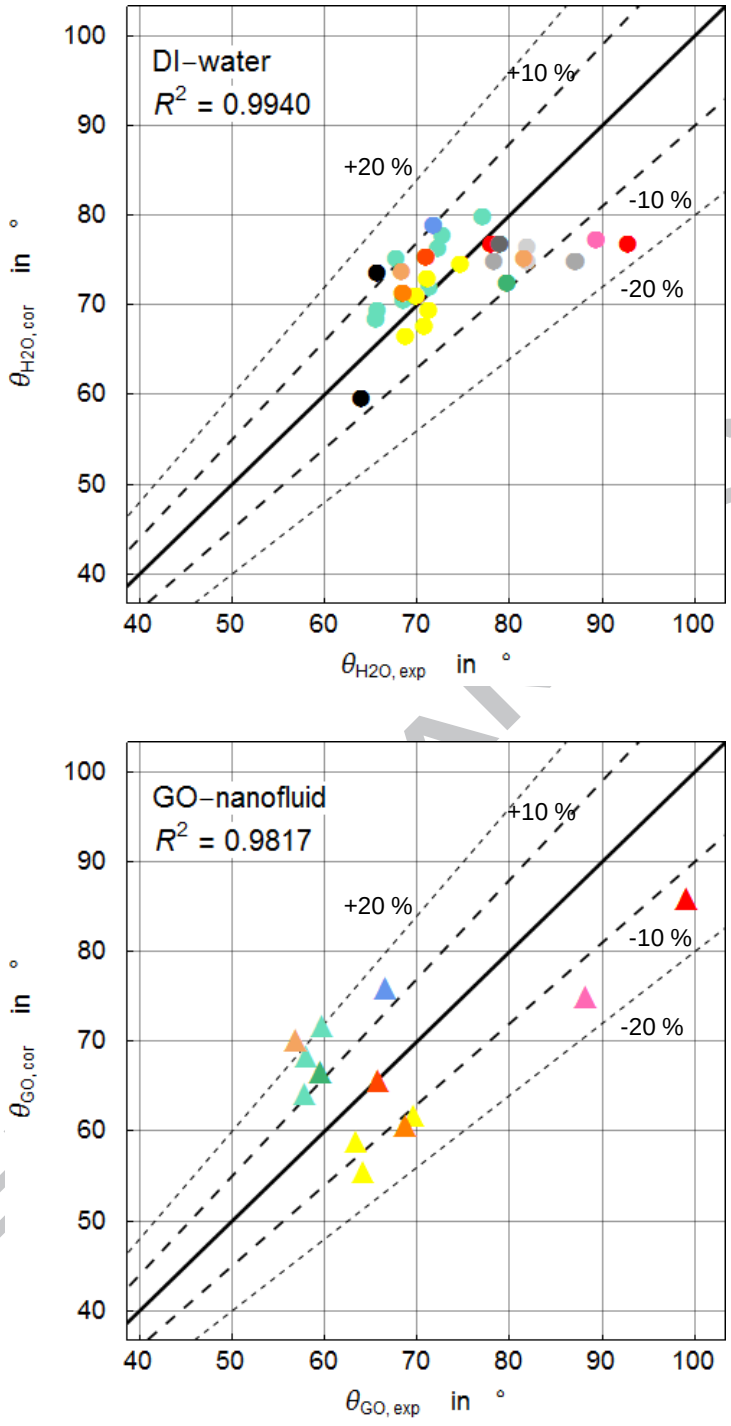

Fig. 7: Comparison of experimental and fitted contact angles according to eq. (1), respectively. Upper plot reference fluid DI-water and lower plot graphene oxide nanofluid. Independent data (upper plot) are indicated by black dots [33], dark grey dot [5], light grey dots [35], and pale grey [34].

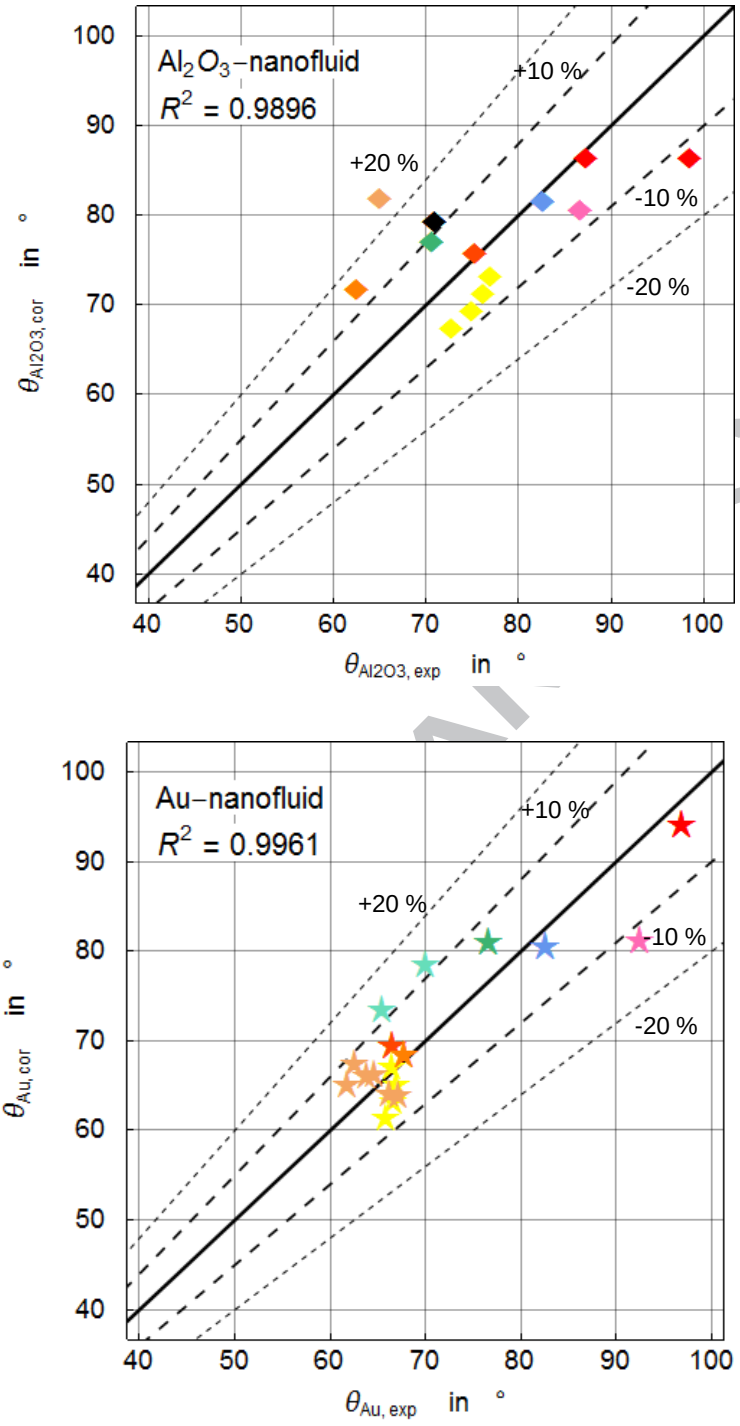

Continuation from previous page.

Upper plot reference alumina nanofluid and lower plot gold nanofluid. Independent data (upper plot) are indicated by a black diamond [5].

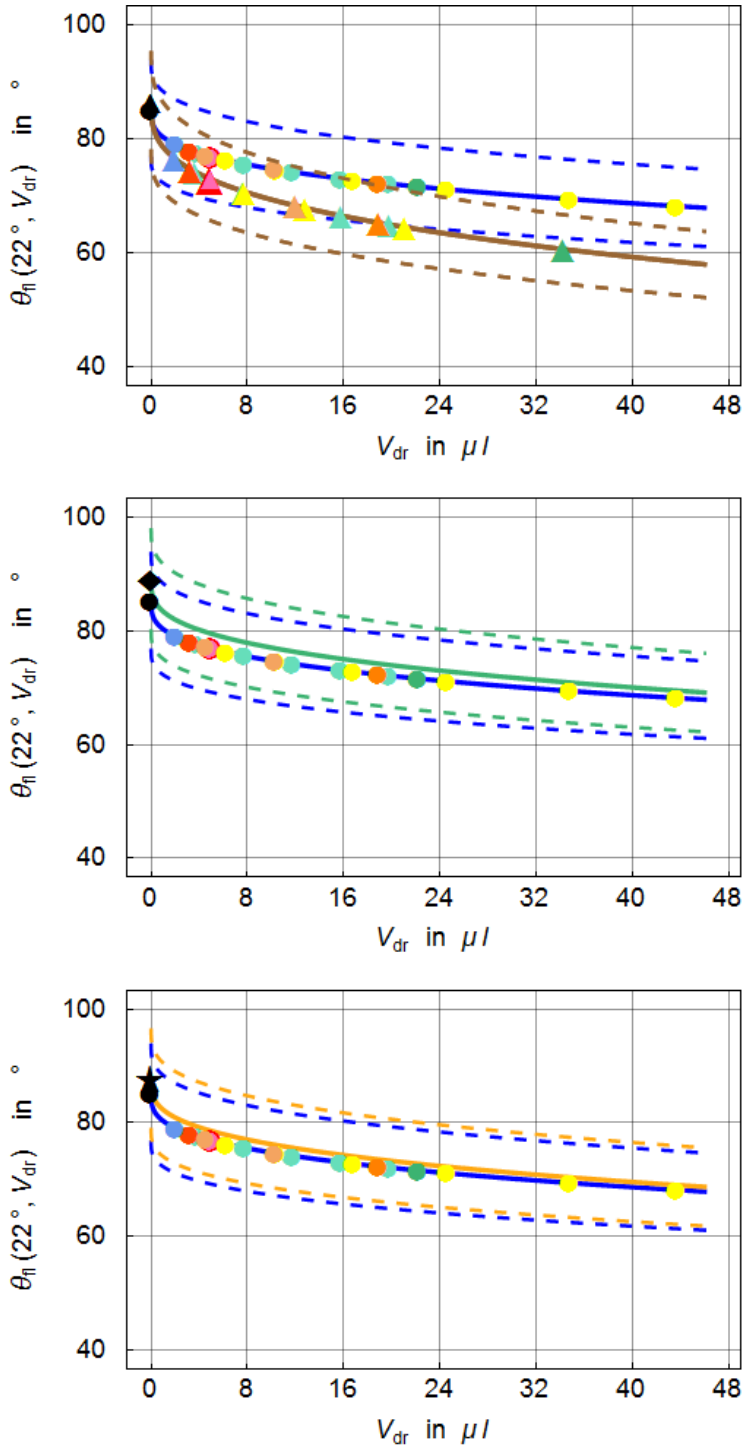

Fig. 8: Replot of experimental data employing the fitting functions for 22 °C. Upper graphene oxide (brown), middle plot alumina nanofluid (green), and lower plot gold nanofluid (yellow). Blue curves indicate water. Full curves show fit at 22 °C and broken curves ±10 % departure.

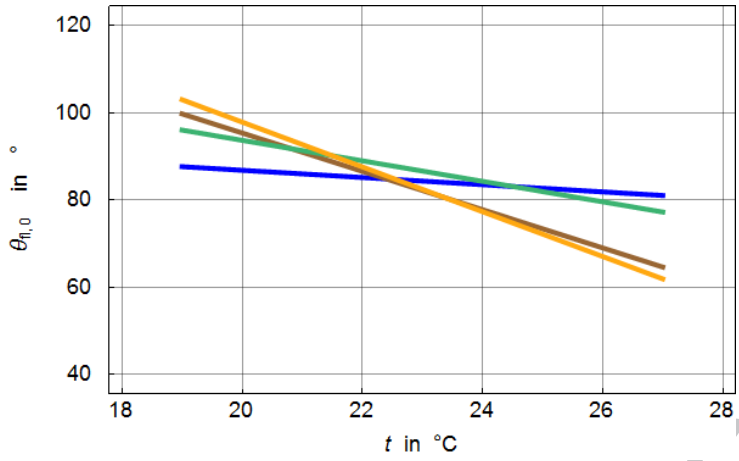

Fig. 9: Limiting contact angle for the zero-volume. Colours indicate: blue – water, brown – graphene oxide, green – alumina nanofluid, and yellow – gold nanofluid.